

Magnetic small-angle neutron scattering by a nanocrystalline ferromagnet with anisotropic exchange interaction

V.D. Zaporozhets  ^a and K.L. Metlov  ^a

^aGalkin Donetsk Institute for Physics and Engineering, 72 R. Luxembourg str., Donetsk, Russia 83114

Synopsis

A micromagnetic framework of magnetic small-angle neutron scattering is developed that incorporates weak symmetric anisotropic exchange and predicts new angular harmonics in magnetic SANS cross sections of polycrystalline ferromagnets.

Abstract

A micromagnetic framework for magnetic small-angle neutron scattering (SANS) is presented that accounts for weak symmetric anisotropic exchange in centrosymmetric nanocrystalline ferromagnets. The exchange interaction is expressed via a general fourth-rank tensor decomposed into isotropic and deviatoric parts. We start with the exchange energy and effective field, assuming weakly fluctuating in space saturation magnetization, solve micromagnetic problem to find spatial distribution of local magnetization vector and compute the averaged (over random orientations of nanocrystals) SANS cross sections. The isotropic part reproduces the classical Heisenberg-type SANS response, while non-zero deviatoric part of the exchange tensor gives rise to new angular harmonics in the magnetic SANS cross section. As a specific example, analytical response functions for an exchange tensor with hexagonal symmetry in perpendicular and parallel scattering geometries are derived. The results provide a basis for identifying and quantifying symmetric exchange anisotropy in magnetic SANS experiments.

Keywords: small-angle neutron scattering; SANS; micromagnetics; anisotropy.

1 Introduction

Magnetic small-angle neutron scattering (SANS) is an experimental technique for characterizing spin textures, magnetic correlations, and magnetization inhomogeneities in nanostructured ferromagnets and magnetic alloys. By analyzing the angular dependence of the scattered intensity in reciprocal space, magnetic SANS provides access to magnetization fluctuations on length scales ranging from a few up to several hundred nanometers (Michels, 2021).

Theoretical description of magnetic SANS is commonly based on micromagnetic continuum theory (Michels, 2014). Within this framework, dominant sources of spin misalignment include

magnetostatic interactions, random magnetic anisotropy, exchange interaction, and spatial variations of saturation magnetization. Micromagnetic theory of magnetic SANS has been successfully applied to a wide range of bulk and nanostructured ferromagnets (Michels, 2021). Several extensions of this theory have been proposed to account for additional effects, such as macroscopic uniaxial anisotropy (Zaporozhets *et al.*, 2022), higher-order terms in the perturbative expansion of the micromagnetic equations (Metlov & Michels, 2015) and effects of the Dzyaloshinskii–Moriya interaction (DMI) (Michels *et al.*, 2019).

In all these approaches, however, the exchange interaction itself is treated within the isotropic Heisenberg approximation, characterized by a single scalar exchange stiffness and the corresponding exchange length. This approximation considerably simplifies the theory and has proven adequate for many applications. Nevertheless, from a microscopic point of view, it is not always justified.

In real magnetic materials, the exchange interaction may acquire a directional dependence primarily through spin–orbit coupling, whose effect is enabled and modulated by reduced lattice symmetry, anisotropic chemical bonding, and local lattice distortions. Such effects are commonly described in terms of anisotropic exchange stiffness. The influence of exchange anisotropy has been investigated in various contexts, including spin-wave dispersion, domain-wall structure, and magnetic phase stability (Belashchenko, 2004; Toga *et al.*, 2018). In the context of magnetic SANS, anisotropic exchange is expected to modify the angular dependence of the scattering cross section and to generate angular harmonics that are absent in the isotropic theory.

At the continuum level, the most general exchange energy density can be written as the sum of two distinct contributions (Akhiezer *et al.*, 1968). The first is an antisymmetric term that is linear in spatial gradients and gives rise to the DMI, which is allowed only in non-centrosymmetric crystals. The second is a symmetric term that is quadratic in gradients and is described by a fourth-rank exchange tensor. Although the influence of DMI on magnetic SANS has been discussed in several recent studies (Michels *et al.*, 2019; Quan *et al.*, 2020), the role of symmetric anisotropic exchange has received comparatively little attention. In centrosymmetric ferromagnets, where DMI is forbidden by symmetry, symmetric exchange anisotropy represents the leading correction to the isotropic Heisenberg interaction.

The aim of the present work is to develop a micromagnetic theory of magnetic SANS that consistently accounts for weak symmetric anisotropic exchange in polycrystalline ferromagnets. Starting from a general fourth-rank exchange tensor, we separate the isotropic and deviatoric contributions and derive a compact expression for the effective exchange field that remains valid in the presence of spatially inhomogeneous material parameters. Within a linearized micromagnetic framework, the isotropic part of the exchange tensor reproduces the standard Heisenberg-type SANS response, while all the anisotropic corrections originate from the deviator part of the exchange tensor.

We show that symmetric exchange anisotropy leads to additional angular harmonics in the magnetic SANS cross section, whose structure depends on the symmetry of the exchange tensor and on the scattering geometry. As a specific example, we analyze the case of hexagonal exchange symmetry and derive explicit analytical expressions for the corresponding anisotropic response functions in both perpendicular and parallel scattering geometries. The obtained results provide a framework for identifying and quantifying the effects of weak symmetric exchange anisotropy in magnetic SANS experiments.

2 Magnetic small-angle neutron scattering

For an ordered ferromagnet well below the Curie temperature, the local magnetization satisfies $|\mathbf{M}(\mathbf{r})| = M_S(\mathbf{r})$ and can be written as $\mathbf{M}(\mathbf{r}) = M_S(\mathbf{r}) \mathbf{m}(\mathbf{r})$ with $|\mathbf{m}| = 1$. In a perfectly uniform medium, \mathbf{m} aligns with \mathbf{H} . In real nanostructured materials, defects and spatial variations in material parameters produce spin misalignment, which causes magnetic SANS at finite q .

In a typical magnetic SANS experiment (Michels, 2014), neutrons with incident wave vector \mathbf{k} pass through a sample and are scattered in the direction of an outgoing wave vector \mathbf{k}' . The momentum-transfer vector is

$$\mathbf{q} = \mathbf{k}' - \mathbf{k}. \quad (1)$$

The scattering vector \mathbf{q} selects spatial Fourier components of the magnetization distribution that contribute to the measured intensity.

The total macroscopic (unpolarized) SANS cross section can be decomposed into

$$\frac{d\Sigma}{d\Omega} = \left(\frac{d\Sigma}{d\Omega} \right)_{\text{res}} + \left(\frac{d\Sigma}{d\Omega} \right)_{\text{M}}, \quad (2)$$

where $(d\Sigma/d\Omega)_{\text{res}}$ denotes a field-independent residual (nuclear and magnetic) background, and $(d\Sigma/d\Omega)_{\text{M}}$ is the magnetic spin-misalignment contribution that vanishes in the high-field limit.

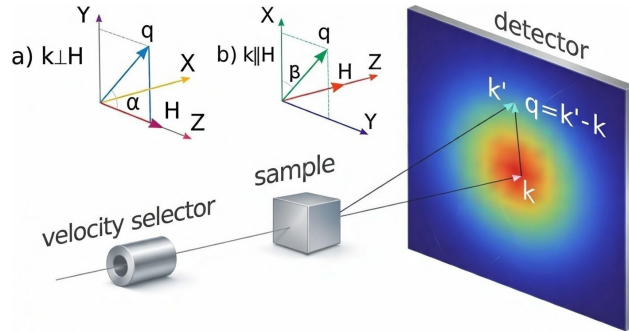


Figure 1: Typical geometry of a magnetic SANS experiment. Neutrons with incident wave vector \mathbf{k} are scattered into the direction \mathbf{k}' , giving rise to the scattering vector $\mathbf{q} = \mathbf{k}' - \mathbf{k}$. The applied magnetic field \mathbf{H} can be oriented either perpendicular or parallel to the beam direction. In the perpendicular geometry, \mathbf{H} is directed along the Z axis, and the detector plane coincides with the Y - Z plane.

Figure 1 shows that magnetic SANS experiments are commonly performed in two scattering geometries: (i) the perpendicular geometry, where the incident neutron beam is oriented perpendicular to the applied magnetic field, $\mathbf{k} \perp \mathbf{H}$, and (ii) the parallel geometry, where $\mathbf{k} \parallel \mathbf{H}$. In both cases, a Cartesian laboratory coordinate system is introduced such that the scattering vector \mathbf{q} lies in the detector plane.

The orientation of \mathbf{q} in the detector plane is conveniently described by its magnitude $q = |\mathbf{q}|$ and an azimuthal angle α or β , measured with respect to the X axis. Consequently, the components of the

dimensionless scattering vector \mathbf{q}/q are expressed as

$$(x_q, y_q, z_q) = \begin{cases} (0, \cos \alpha, \sin \alpha), & \text{perpendicular geometry,} \\ (\cos \beta, \sin \beta, 0), & \text{parallel geometry.} \end{cases}$$

In perpendicular geometry, the unpolarized magnetic spin-misalignment can be written in the following form (Michels, 2014)

$$\frac{d\Sigma_{\text{M}}^{\perp}}{d\Omega} = 8\pi^3 V b_{\text{H}}^2 \left(|\widetilde{M}_X|^2 + |\widetilde{M}_Y|^2 \cos^2 \alpha + (|\widetilde{M}_Z|^2 - |\widetilde{M}_S|^2) \sin^2 \alpha - \Re\{\widetilde{M}_Y \widetilde{M}_Z^*\} \sin 2\alpha \right), \quad (3)$$

where V is the scattering volume, b_{H} is the magnetic scattering length per Bohr magneton, and $\widetilde{M}_{X,Y,Z}(\mathbf{q})$ are Fourier components of the magnetization. In Eq. (3), $\Re\{\dots\}$ denotes the real part and the superscript $*$ indicates the complex conjugation.

In the parallel geometry, the corresponding unpolarized magnetic spin-misalignment cross section reads

$$\frac{d\Sigma_{\text{M}}^{\parallel}}{d\Omega} = 8\pi^3 V b_{\text{H}}^2 \left(|\widetilde{M}_X|^2 \sin^2 \beta + |\widetilde{M}_Y|^2 \cos^2 \beta + (|\widetilde{M}_Z|^2 - |\widetilde{M}_S|^2) - \Re\{\widetilde{M}_X \widetilde{M}_Y^*\} \sin 2\beta \right). \quad (4)$$

Magnetic small-angle neutron scattering experiments can be performed in various scattering geometries depending on the relative orientation of the applied magnetic field, the incident neutron beam, and the detector plane. In the present work, however, we restrict ourselves to the two experimentally relevant geometries mentioned above.

The Fourier transform convention used throughout this work is

$$\widetilde{F}(\mathbf{q}) = \frac{1}{V} \int_V F(\mathbf{r}) e^{-i\mathbf{q}\cdot\mathbf{r}} d^3r, \quad F(\mathbf{r}) = \sum_{\mathbf{q}} \widetilde{F}(\mathbf{q}) e^{i\mathbf{q}\cdot\mathbf{r}}. \quad (5)$$

Equations (3)–(5) show that the central theoretical task is to compute the Fourier components \widetilde{M}_X , \widetilde{M}_Y , and \widetilde{M}_Z from a micromagnetic model. In the following sections, we formulate the exchange energy in a general tensorial form and derive the corresponding effective field and its Fourier representation, which provides the starting point for the linearized Brown equations and for the analytical calculation of magnetic SANS response functions in both scattering geometries.

3 Symmetric anisotropic exchange energy

In a centrosymmetric ferromagnet, the most general continuum exchange energy density that is quadratic in spatial derivatives of the magnetization can be written in tensorial form (Akhiezer *et al.*, 1968) as

$$e_{\text{EX}} = \frac{1}{2} \sum_{\alpha\beta\gamma\delta} C_{\alpha\beta\gamma\delta} \partial_{\beta} m_{\alpha} \partial_{\delta} m_{\gamma}, \quad (6)$$

where Greek indices denote Cartesian components, $\partial_{\alpha} \equiv \partial/\partial x_{\alpha}$, and $C_{\alpha\beta\gamma\delta}$ is a fourth-rank exchange tensor. The tensor is symmetric with respect to the index pairs (α, β) and (γ, δ) and reflects the symmetry of the crystal point group. This approach unifies various possible symmetries within a single framework. The components $C_{\alpha\beta\gamma\delta}$ quantitatively determine how the change in the

magnetization component m_α along the x_β direction is related to the change in m_γ along x_δ . For an isotropic ferromagnet, the tensor reduces to

$$C_{\alpha\beta\gamma\delta} = C \delta_{\alpha\gamma} \delta_{\beta\delta}, \quad (7)$$

where C is the conventional scalar exchange stiffness. In the general case, $C_{\alpha\beta\gamma\delta}$ contains both isotropic and anisotropic contributions.

In nanostructured ferromagnets, saturation magnetization $M_S(\mathbf{r})$ and exchange constant $C(\mathbf{r})$ may vary spatially due to compositional fluctuations or multiphase microstructure. We introduce (Michels, 2021)

$$M_S(\mathbf{r}) = M_0 (1 + I_M(\mathbf{r})), \quad |I_M| \ll 1, \quad (8)$$

where I_M describes its weak inhomogeneities and is zero on average $\langle I_M \rangle = 0$. Using a derivative operator (see the Appendix A for definition) that takes into account the inhomogeneity of M_S :

$$\mathcal{D}_\beta M_\alpha = \partial_\beta M_\alpha - M_\alpha \partial_\beta \ln \frac{M_S}{M_0}, \quad (9)$$

makes it possible to compactly write down the exchange energy as

$$e_{\text{EX}}(\mathbf{r}) = \frac{\gamma_B}{2M_S^2} \sum_{\alpha,\beta,\gamma,\delta} C_{\alpha\beta\gamma\delta}(\mathbf{r}) (\mathcal{D}_\beta M_\alpha) (\mathcal{D}_\delta M_\gamma). \quad (10)$$

This form is particularly useful for deriving the effective exchange field via functional differentiation.

4 Effective exchange field

From the effective field definition, calculating all the derivatives and using the symmetry of the tensor $C_{\alpha\beta\gamma\delta}$, we obtain (see the Appendix B for details) a compact expression

$$H_{\text{EX},\alpha} = \frac{\gamma_B}{\mu_0} [\partial_\beta T_{\alpha\beta} + (\partial_\beta \ln M_S) T_{\alpha\beta}], \quad (11)$$

where the quantity

$$T_{\alpha\beta} = \frac{C_{\alpha\beta\gamma\delta}}{M_S^2} \mathcal{D}_\delta M_\gamma \quad (12)$$

is conceptually similar to a stress tensor in elasticity theory. The factor γ_B is introduced (Aharoni, 1996) to conveniently account for different possible systems of magnetic units. For example, in the SI system μ_0 denotes the permeability of vacuum and $\gamma_B = 1$, whereas in the CGS system $\mu_0 = 1$ and $\gamma_B = 4\pi$.

Having obtained the general formula for the effective exchange field, we proceed to calculate its Fourier transform, which is necessary for further derivation of the angular dependences of the magnetic SANS cross sections. The key step here is to expand the quantity $T_{\alpha\beta}$ in terms of smallness of $I_M(\mathbf{r})$ and isolate only those terms that contribute in the first order of perturbation theory.

Expanding the expression $1/M_S^2$ up to the first order in saturation magnetization fluctuations

$$\frac{1}{M_S^2} = \frac{1}{M_0^2} (1 - 2I_M) = \frac{1}{M_0^2} + O(I_M), \quad (13)$$

and substituting it in (12) together with (8) inside the functional derivative \mathcal{D}_β , we obtain:

$$T_{\alpha\beta} = \frac{C_{\alpha\beta\gamma\delta}}{M_s^2} \mathcal{D}_\delta M_\gamma = \frac{C_{\alpha\beta\gamma\delta}}{M_0^2} (\partial_\delta M_\gamma - M_\gamma \partial_\delta I_M) + O(I_M^2). \quad (14)$$

Now, let us treat the transversal and longitudinal components separately. For $\gamma = Z$:

$$\partial_\delta M_Z = M_0 \partial_\delta I_M, \quad \Rightarrow \quad \mathcal{D}_\delta M_Z = M_0 \partial_\delta I_M - M_0(1 + I_M) \partial_\delta I_M = O(I_M^2). \quad (15)$$

That is, the longitudinal part completely disappears in the first order.

For $\gamma = X, Y$:

$$\mathcal{D}_\delta M_{X,Y} = \partial_\delta M_{X,Y}^{(1)} - M_{X,Y}^{(1)} \partial_\delta I_M, \quad (16)$$

where $M_{X,Y}^{(1)}$ are magnetization components that are of the same order as I_M . Since the second term contains the product of two small quantities, it is of the second order and is discarded:

$$\mathcal{D}_\delta M_{X,Y} \approx \partial_\delta M_{X,Y}^{(1)} \quad (17)$$

Taking these expressions into account, we can write the following formula for $T_{\alpha\beta}$

$$T_{\alpha\beta} = \frac{C_{\alpha\beta\gamma\delta}}{M_0^2} \partial_\delta M_\gamma. \quad (18)$$

Thus, the expression for the effective exchange field in the first order takes the form

$$H_{\text{EX},\alpha} = \frac{1}{\mu_0} \partial_\beta T_{\alpha\beta} = \frac{1}{\mu_0 M_0^2} C_{\alpha\beta\gamma\delta} \partial_\beta \partial_\delta M_\gamma. \quad (19)$$

To get the expressions for transverse magnetization components, one needs to compute the Fourier image of the above effective field. Using $\partial_\beta \rightarrow iq_\beta$, we have

$$\tilde{H}_{\text{EX},\alpha} = \frac{1}{\mu_0 M_0^2} C_{\alpha\beta\gamma\delta} (iq_\beta) (iq_\delta) \tilde{M} = -\frac{1}{\mu_0 M_0^2} C_{\alpha\beta\gamma\delta} q_\beta q_\delta \tilde{M}. \quad (20)$$

Let us introduce a matrix $K_{\alpha\gamma}$

$$K_{\alpha\gamma}(\mathbf{q}) = \frac{1}{\mu_0 M_0^2} C_{\alpha\beta\gamma\delta} q_\beta q_\delta, \quad (21)$$

to represent the effective field in a compact form:

$$\tilde{H}_{\text{EX},\alpha} = -K_{\alpha\gamma}(\mathbf{q}) \tilde{M}_\gamma. \quad (22)$$

This representation is especially convenient, since all the exchange contributions enter the linearized Brown's equations exclusively through the matrix $K_{\alpha\gamma}(\mathbf{q})$. As a result, the influence of the anisotropic exchange on the magnetic response is entirely governed by the tensorial structure of $K(\mathbf{q})$. Because the exchange tensor $C_{\alpha\beta\gamma\delta}$ is symmetric with respect to the permutations of index pairs, $K_{\alpha\gamma}(\mathbf{q})$ is a real symmetric matrix for each fixed \mathbf{q} .

5 Deviatoric part of the exchange tensor

Now we decompose the tensor $C_{\alpha\beta\gamma\delta}$ into the diagonal part and the deviator:

$$C_{\alpha\beta\gamma\delta} = C_0 \delta_{\alpha\gamma} \delta_{\beta\delta} + \xi D_{\alpha\beta\gamma\delta}, \quad (23)$$

where ξ is a small parameter, and $\text{Tr}(D) = 0$. The contribution of the isotropic part to the K function gives

$$K_{\alpha\gamma}^{(0)}(q) = \frac{1}{\mu_0 M_0^2} C_0 q^2 \delta_{\alpha\gamma} = \gamma_B L_0^2 q^2 \delta_{\alpha\gamma}, \quad (24)$$

where $L_0 = \sqrt{2C/(\gamma_B \mu_0 M_0^2)}$ is the exchange length. The anisotropic contribution has the form

$$\Delta K_{\alpha\gamma}(q) = \frac{1}{\gamma_B \mu_0 M_0^2} D_{\alpha\beta\gamma\delta} q_\beta q_\delta. \quad (25)$$

These expressions are currently written in a coordinate system associated with the crystallite. However, in a polycrystalline ferromagnet, each grain has a random orientation of its crystallographic axes, which, as a rule, do not coincide with the orientation of the laboratory frame, defined by the direction of the external magnetic field and the neutron beam.

After the isotropic and deviatoric parts of the exchange tensor are separated, it becomes possible to write down the effective field in the laboratory coordinate system and clearly trace which combinations of tensor components and fluctuations of magnetic quantities determine the angular dependence of the magnetic cross sections of SANS. Let the rotation of an individual grain relative to the laboratory system be given by the Euler matrix $\mathcal{R}(\phi, \theta, \psi)$. Then the transition from crystallographic indices $(\alpha\beta\gamma\delta)$ to laboratory indices $(ijkl)$ is carried out according to the standard rule:

$$C_{ijkl}^{(R)} = \mathcal{R}_{i\alpha} \mathcal{R}_{j\beta} \mathcal{R}_{k\gamma} \mathcal{R}_{l\delta} C_{\alpha\beta\gamma\delta}. \quad (26)$$

Substituting this expression into the isotropic part of the function $K_{\alpha\gamma}(q)$, we obtain:

$$K_{ij}^{(0)}(q) = \mathcal{R}_{i\alpha} \mathcal{R}_{j\gamma} K_{\alpha\gamma}^{(0)}(q) = C_0 q^2 \mathcal{R}_{i\alpha} \mathcal{R}_{j\gamma} \delta_{\alpha\gamma} = C_0 q^2 \delta_{ij}. \quad (27)$$

Thus, the isotropic contribution takes the same form in any coordinate system. Physically, this means that ordinary (scalar) exchange is independent of the crystal lattice orientation. For the deviatoric part, we have:

$$\Delta K_{ij}(q) = \mathcal{R}_{i\alpha} \mathcal{R}_{j\beta} \mathcal{R}_{k\gamma} \mathcal{R}_{l\delta} D_{\alpha\beta\gamma\delta} q_k q_l \quad (28)$$

where the indices for \mathbf{q} are changed to the laboratory frame because only the tensor $D_{\alpha\beta\gamma\delta}$ must be rotated, whereas \mathbf{q} remains fixed. This way, the expression for K becomes

$$\Delta K_{ij}(q) = \mathcal{R}_{i\alpha} \mathcal{R}_{j\gamma} \Delta K_{\alpha\gamma}(q), \quad (29)$$

and the effective exchange field assumes its final form:

$$\tilde{H}_{\text{EX},i} = -\gamma_B \left[K_{ij}^{(0)} + \xi \Delta K_{ij} \right] \tilde{M}_j^{(1)}(q), \quad (30)$$

where ΔK_{ij} includes all the effects of symmetric exchange in the first order of the small parameter ξ .

The components of the resulting expression can be written explicitly:

$$\tilde{H}_{\text{EX},i} = -\gamma_B \left[L_0^2 q^2 \tilde{M}_i^{(1)} + \xi \left(\Delta K_{iX} \tilde{M}_X^{(1)} + \Delta K_{iY} \tilde{M}_Y^{(1)} + \Delta K_{iZ} \tilde{I}_M \right) \right], \quad (31)$$

where \tilde{I}_M is the Fourier transform of the inhomogeneity function. These expressions show that the appearance of exchange anisotropy leads to new types of connection between transverse and longitudinal magnetization fluctuations. Terms of the form

$$\Delta K_{XZ} \tilde{I}_M, \quad \Delta K_{ZX} \tilde{M}_X^{(1)}, \quad \Delta K_{YZ} \tilde{M}_Y^{(1)}, \quad (32)$$

form new angular dependencies in magnetic SANS cross sections.

Thus, the exchange tensor deviator plays the role of a source of anisotropy in magnetic SANS, and the observed scattering pattern reflects the averaged over all orientations of crystallites effect of these corrections.

6 Brown's equations

Substituting the expressions obtained for the effective exchange field, together with the contributions of the remaining micromagnetic interactions (Metlov & Michels, 2015), into the Brown equations and solving them to first order in the small parameters, we obtain the following expressions for the magnetization components in Fourier space:

$$\tilde{m}_X^{(1)} = \frac{(\tilde{A}_X - \tilde{I}_M x_q y_q + \tilde{I}_M \Delta K_{XZ} \xi) G_Y + X_q (\tilde{I}_M x_q z_q - \tilde{I}_M \Delta K_{YZ} \xi - \tilde{A}_Y)}{(h_q + x_q^2 - \Delta K_{XX} \xi)(h_q + y_q^2 - \Delta K_{YY} \xi) - (x_q y_q - \Delta K_{XY} \xi)^2}, \quad (33)$$

$$\tilde{m}_Y^{(1)} = \frac{(\tilde{A}_Y - \tilde{I}_M x_q y_q + \tilde{I}_M \Delta K_{YZ} \xi) G_X + X_q (\tilde{I}_M y_q z_q - \tilde{I}_M \Delta K_{XZ} \xi - \tilde{A}_X)}{(h_q + y_q^2 - \Delta K_{YY} \xi)(h_q + x_q^2 - \Delta K_{XX} \xi) - (x_q y_q - \Delta K_{XY} \xi)^2}. \quad (34)$$

Here $h_q = h + L_0^2 q^2$, and the contribution of random magnetic anisotropy is represented by the quantities $\tilde{A}_{X,Y} = u_{X,Y} \tilde{Q}_r$, where \tilde{Q}_r is the Fourier transform of the random anisotropy quality factor, which is assumed to be of the same order of smallness as I_M . For the case of random uniaxial anisotropy, the coefficients are given by $u_{X,Y} = d_{X,Y} d_Z$, where $d_{X,Y,Z}(\mathbf{r})$ are unit vectors along the local anisotropy axes.

For compactness, we have introduced the auxiliary quantities

$$G_X = h_q + x_q^2 - \Delta K_{XX} \xi, \quad G_Y = h_q + y_q^2 - \Delta K_{YY} \xi, \quad (35)$$

and

$$X_q = x_q y_q - \Delta K_{XY} \xi. \quad (36)$$

The expressions above for $\tilde{m}_X^{(1)}$ and $\tilde{m}_Y^{(1)}$ constitute the central result required for the calculation of magnetic small-angle neutron scattering cross sections. In order to obtain observable macroscopic quantities in a polycrystalline sample, these expressions must be averaged over the crystallite orientations. This requires averages of various tensor and vector products, such as $\langle A_{X/Y} \Delta K_{ij} \rangle$ and $\langle \Delta K_{ij} \rangle$. They depend explicitly on the symmetry of the exchange tensor, or, more precisely, on the symmetry of its deviatoric part and on the chosen scattering geometry. Owing to the smallness of the anisotropy parameter ξ , this averaging procedure can be carried out perturbatively.

Substituting the expressions for the transverse components of the magnetization (33) and (34) into the formula for the perpendicular magnetic SANS cross section and expanding in powers of ξ , the cross section can be split into two parts

$$\frac{d\Sigma_{\perp}^M}{d\Omega} = \frac{d\Sigma_{\perp}^M}{d\Omega} \Big|_{HEIS} + \frac{d\Sigma_{\perp}^M}{d\Omega} \Big|_A, \quad (37)$$

where the first term corresponds to the well-known Heisenberg-type exchange contribution (Michels, 2021), while the second term represents the anisotropic corrections.

The anisotropic contribution can be further expanded into a series over the small parameter ξ ,

$$\frac{d\Sigma_{\perp}^M}{d\Omega} \Big|_A = \frac{d\Sigma_{\perp}^M}{d\Omega} \Big|_{\xi} + \frac{d\Sigma_{\perp}^M}{d\Omega} \Big|_{\xi\kappa} + \frac{d\Sigma_{\perp}^M}{d\Omega} \Big|_{\xi^2} + \dots \quad (38)$$

The leading anisotropic contribution, linear in ξ , takes the form

$$\frac{d\Sigma_{\perp}^M}{d\Omega} \Big|_{\xi} = \frac{8\pi^3}{V} b_H^2 M_0^2 \tilde{I}_M^2 \xi \frac{2y_q z_q (h_q + 1) (K_{YY} y_q z_q - K_{YZ} (h_q + y_q^2))}{(h_q + y_q^2)^3}. \quad (39)$$

The mixed contribution proportional to $\kappa\xi$ can be written in a compact form as a scalar product of two vectors, $\mathbf{u} = (u_X, u_Y)$ and $\Phi = (\Phi_X, \Phi_Y)$,

$$\frac{d\Sigma_{\perp}^M}{d\Omega} \Big|_{\kappa\xi} = \frac{8\pi^3}{V} b_H^2 M_0^2 \tilde{I}_M^2 \kappa\xi (\mathbf{u} \cdot \Phi), \quad (40)$$

where the components of the vector Φ are given by

$$\Phi_X = -\frac{2K_{YY} y_q z_q}{(h_q + y_q^2)^2} + \frac{2h_q K_{YZ} z_q^2}{(h_q + y_q^2)^3} + \frac{2K_{YY} y_q^2 z_q^2}{(h_q + y_q^2)^3} - \frac{4K_{YY} y_q z_q^3}{(h_q + y_q^2)^3}, \quad (41)$$

$$\begin{aligned} \Phi_Y &= \frac{2K_{XZ}}{h_q^2} - \frac{2K_{XY} y_q z_q}{(h_q + y_q^2)^2} - \frac{2K_{XY} y_q z_q}{h_q (h_q + y_q^2)^2} - \frac{2K_{XY} y_q^3 z_q}{h_q^2 (h_q + y_q^2)} \\ &\quad - \frac{2K_{XY} y_q z_q^3}{(h_q + y_q^2)^3} - \frac{2K_{XY} y_q^3 z_q^3}{h_q (h_q + y_q^2)^3}. \end{aligned} \quad (42)$$

The full expression for the contribution quadratic in ξ is lengthy and is therefore relegated to Appendix D.

It is important to emphasize that the parameters ξ and κ play fundamentally different roles in the present theory and are therefore treated differently. The parameter ξ measures the relative strength of the symmetric anisotropic part of the exchange tensor with respect to its isotropic component. Since symmetric exchange anisotropy originates from spin-orbit coupling, it is generally much weaker than the dominant Heisenberg exchange, which justifies a systematic expansion in the powers of ξ .

In contrast, the parameter κ relates the random magnetic anisotropy quality factor to the general inhomogeneity function $I_M(\mathbf{r})$ that describes spatial variations of magnetic material parameters. It does not represent an independent small interaction, but rather characterizes how random anisotropy

couples to existing magnetization inhomogeneities. As a result, κ is treated on the same footing as other sources of spin misalignment present in isotropic micromagnetic theory and is not used as an expansion parameter. The terms proportional to $\xi\kappa$ therefore describe the leading coupling between weak symmetric exchange anisotropy and random-anisotropy-induced spin disorder.

In order to obtain explicit angular dependencies, it is necessary to specify the symmetry of the tensor $C_{\alpha\beta\gamma\delta}$ and to perform the corresponding averaging of the expressions entering $d\Sigma^M/d\Omega|_A$. In the present work, we investigate the influence of hexagonal exchange on the magnetic SANS cross sections.

7 Hexagonal symmetry of the exchange tensor

The number of independent exchange parameters is determined by the crystallographic point symmetry acting on the fourth-rank exchange tensor $C_{\alpha\beta\gamma\delta}$. The higher the crystal symmetry, the smaller the number of independent coefficients; conversely, a lower symmetry allows for a larger number of distinct exchange stiffnesses. In the present section, we restrict ourselves to the conventional minimal representation of hexagonal symmetry, which captures the dominant anisotropic effects while preserving analytical transparency of the model.

In the crystallite coordinate system (X', Y', Z') , the hexagonal axis is directed along Z' . In this coordinate system, the deviatoric part of the hexagonal symmetry exchange tensor takes the form:

$$D_{\alpha\beta\gamma\delta} = \delta_{\alpha\gamma} \Delta C \left(n_\beta n_\delta - \frac{1}{3} \delta_{\beta\delta} \right), \quad (43)$$

where $\Delta C = C_Z - C_\perp$ is the difference between the longitudinal and transverse exchange constants, and $n_\alpha = \delta_{\alpha Z}$ are the components of the unit vector $\mathbf{n} = (0, 0, 1)$ along the hexagonal axis.

Substituting this expression into the definition of the deviatoric part of the kernel (25), one obtains for the hexagonal symmetry

$$\Delta K_{\alpha\gamma} = \delta_{\alpha\gamma} \Delta C \left[(\mathbf{n} \cdot \mathbf{q})^2 - \frac{1}{3} q^2 \right], \quad (44)$$

where the dot denotes the scalar product.

In order to obtain the expression for $\Delta K_{\alpha\gamma}$ in the laboratory coordinate system, the tensor $D_{\alpha\beta\gamma\delta}$ is transformed using the rotation matrix \mathcal{R} ,

$$D_{ijkl}^{(R)} = \mathcal{R}_{i\alpha} \mathcal{R}_{j\beta} \mathcal{R}_{k\gamma} \mathcal{R}_{l\delta} D_{\alpha\beta\gamma\delta} = \Delta C \mathcal{R}_{i\alpha} \mathcal{R}_{j\beta} \mathcal{R}_{k\gamma} \mathcal{R}_{l\delta} \delta_{\alpha\gamma} \left(n_\beta n_\delta - \frac{1}{3} \delta_{\beta\delta} \right). \quad (45)$$

Using the orthogonality relations $\mathcal{R}_{i\alpha} \mathcal{R}_{j\alpha} = \delta_{ij}$ and $\hat{R}_{k\beta} \mathcal{R}_{l\beta} = \delta_{kl}$, one obtains

$$D_{ijkl}^{(R)} = \Delta C \delta_{ij} \left(n_k n_l - \frac{1}{3} \delta_{kl} \right), \quad (46)$$

which has the same structure as in the crystallite coordinate system, but now with $\mathbf{n} = (n_X, n_Y, n_Z)$ expressed through laboratory coordinates.

Substituting the expression for $D_{ijkl}^{(R)}$ into the formula for ΔK_{ik} , we get the following expression for

the deviatoric part of the kernel K in the laboratory coordinate system:

$$\Delta K_{ik} = \Lambda_q^2 \left[(\mathbf{n} \cdot \mathbf{q})^2 - \frac{1}{3} q^2 \right] n_i n_k, \quad (47)$$

where

$$\Lambda_q^2 = \frac{\Delta C}{\mu_0 \gamma_B M_0^2}. \quad (48)$$

To obtain expressions for perpendicular cross sections, one needs to substitute expressions for $\Delta K_{ij}^{(R)}$ into (3) and carry out averaging procedure.

7.1 Magnetic SANS in the presence of hexagonal exchange

The averaging procedure required to obtain macroscopic magnetic SANS cross sections consists of two steps: averaging over realizations of structural inhomogeneities (Metlov & Michels, 2015), and averaging over the orientations of crystallites in a polycrystalline sample. The latter reduces to evaluating the averages of combinations such as $\langle \Delta K_{XY}^{(R)} u_X(\mathbf{q}) \rangle$. In the following, we assume that the directions of the hexagonal exchange axis and the uniaxial anisotropy axis coincide. Expressing the unit vectors \mathbf{n} and \mathbf{d} through the same set of spherical angles and performing the corresponding angular integrations yields the averaged scattering cross sections.

Following the formulation introduced in (Michels, 2014), the anisotropic part of the perpendicular magnetic SANS cross section can be written as

$$\left. \frac{d\Sigma_{\perp}^M}{d\Omega} \right|_A = S_{\xi} R_{\xi} + S_{\xi\kappa} R_{\xi\kappa} + S_{\xi^2} R_{\xi^2} + \dots, \quad (49)$$

where $R(\mathbf{q}, h_q)$ are referred to as response functions and $S(q)$ are the corresponding scattering functions.

Response function R_{ξ}

Retaining only the linear terms in the exchange anisotropy parameter ξ , one obtains the response function

$$R_{\xi} = -\frac{(h_q + 1)(1 + 3h_q) \sin^2 2\alpha}{(h_q + \sin^2 \alpha)^3}, \quad (50)$$

with the associated scattering function $S_{\xi} = \Lambda_q^2 \langle \tilde{I}_M^2 \rangle q^2 \xi / 45$, where $\langle \tilde{I}_M^2 \rangle$ is the averaged Fourier image of the inhomogeneity function (Metlov & Michels, 2015)

To visualize the angular and field dependence of R_{ξ} , we consider two-dimensional plots in the variables α and h_q . Since h_q varies from zero to infinity, we introduce the transformation $h_q = t/(1-t)$, which maps the entire field range to the interval $t \in [0, 1)$. Moreover, because R_{ξ} decays as $1/h_q$ at large fields, we plot the rescaled quantity $h_q(t) R_{\xi}(h_q(t), \mathbf{q})$.

As shown in Fig. 2, the response function R_{ξ} exhibits several characteristic features. The numerator $\sin^2(2\alpha)$ enforces exact zeros at $\alpha = 0, \pi/2$, and π , resulting in vertical nodal lines in the detector plane. The response reaches its maximum at $\alpha = \pi/4$ and $3\pi/4$, leading to two symmetric intensity lobes.

The denominator $(h_q + \sin^2 \alpha)^3$ produces a strong enhancement at small h_q , indicating that the linear

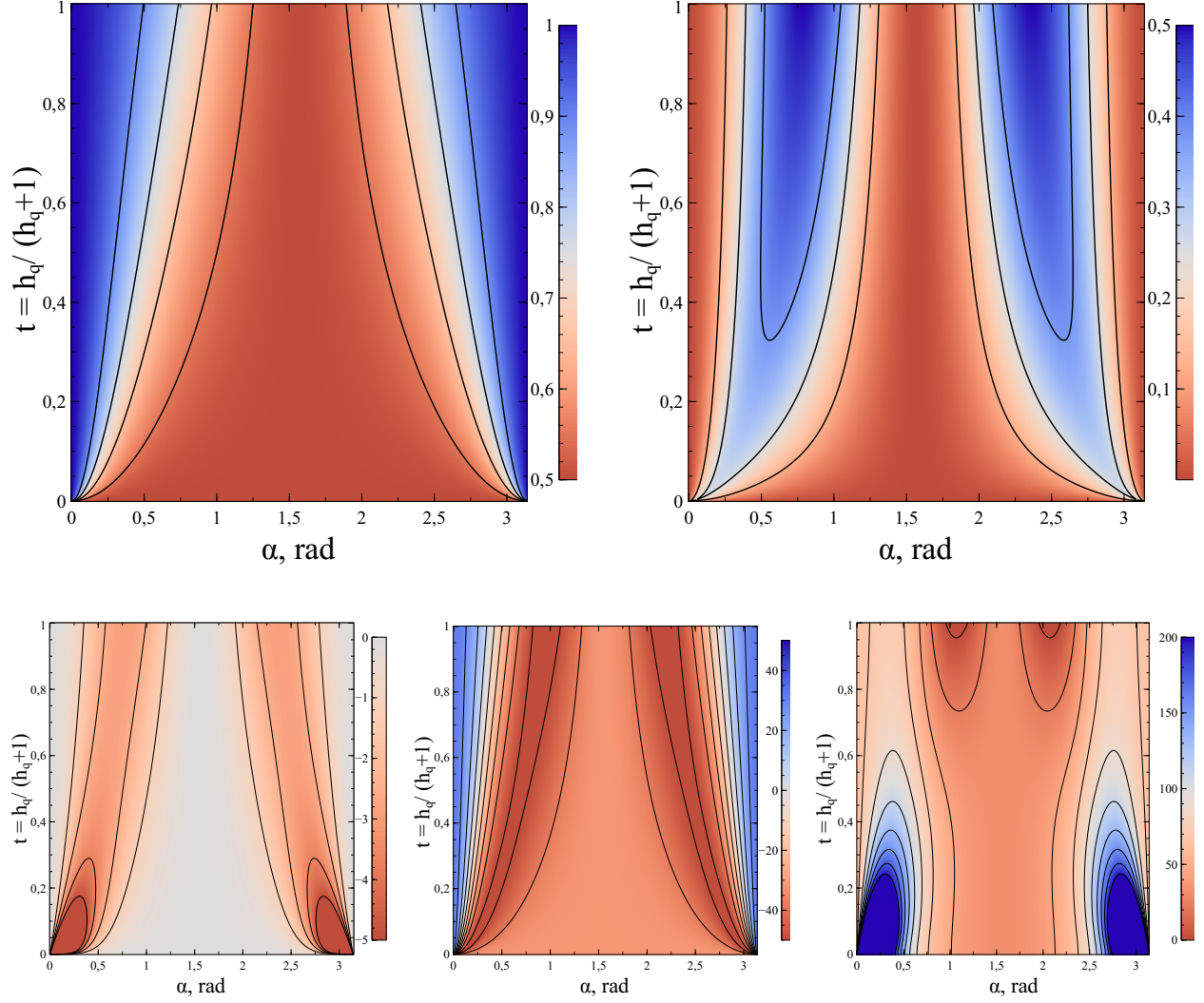


Figure 2: Two-dimensional maps in coordinates of $t = h_q/(h_q + 1)$ and α of the standard (top row: $h_q^2 R_H$ and $h_q R_M$) and hexagonal-exchange-induced (bottom row: $h_q R_\xi$, $h_q^2 R_{\xi\kappa}$ and $h_q^2 R_{\xi 2}$) response functions multiplied by a corresponding power of h_q to compensate for the decay at high fields.

symmetric-exchange contribution is primarily a low-field effect. The function remains negative for all physical h_q , since $(1 + h_q)(1 + 3h_q) > 0$. It is important to emphasize, that although the anisotropic response functions may assume negative values in certain regions of the (α, h_q) parameter space, the total magnetic SANS cross section remains strictly positive for all angles and for all physically relevant values of the model parameters. This reflects the fact that the anisotropic contributions enter as corrections to the dominant isotropic background and do not violate the fundamental positivity of the scattering intensity.

The angular dependence of R_ξ is strictly symmetric with respect to the angles $\pi/2$ and $3\pi/2$. The response reaches its maximum values at $\alpha = \pi/4$ and $3\pi/4$, which can be traced back to the dominant high-field angular contribution $\sin^2 2\alpha$. In addition, R_ξ vanishes at $\alpha = 0, \pi/2, \pi$, and 2π . These zeros become particularly transparent when the response function is plotted as a one-dimensional function of α at fixed h_q .

Response function $R_{\xi\kappa}$

After performing the directional averaging of the mixed $\xi\kappa$ contribution, the response function in this order can be expressed as a finite series of even Fourier harmonics,

$$R_{\xi\kappa} = \frac{1}{h_q^2(h_q + \sin^2 \alpha)^3} \left(\chi_{\kappa\xi}^{(0)} + \chi_{\kappa\xi}^{(2)} \cos 2\alpha + \chi_{\kappa\xi}^{(4)} \cos 4\alpha + \chi_{\kappa\xi}^{(6)} \cos 6\alpha \right), \quad (51)$$

with the corresponding scattering function

$$S_{\xi\kappa} = \frac{\Lambda_q^2}{1260} \langle \tilde{I}_M^2 \rangle q^2 \kappa \xi. \quad (52)$$

The coefficients $\chi_{\kappa\xi}^{(n)}$ are polynomials of second or third order in h_q , their explicit expressions are listed in Appendix C.

The two-dimensional representation of the rescaled response function $h_q(t)^2 R_{\xi\kappa}(h_q(t), \mathbf{q})$, shown in Fig. 2, reveals a distinctive feature absent in R_ξ . In contrast to the latter, the mixed response function $R_{\xi\kappa}$ undergoes a sign reversal along a nontrivial angle–field curve $N(\alpha, h_q) = 0$. This field-dependent nodal structure originates from the mutual cancellation of several competing angular harmonics and constitutes a characteristic signature of the $\xi\kappa$ contribution. This behavior is qualitatively different from that of the standard response functions discussed in (Michels, 2014).

Although harmonics up to $\cos 6\alpha$ formally enter the numerator, the resulting angular variation remains smooth across the detector plane. This behavior demonstrates that higher-order harmonics are efficiently suppressed by the denominator and do not generate rapid angular oscillations in the observable scattering pattern.

Response function R_{ξ^2}

After averaging the part of the cross section that is quadratic in the exchange anisotropy (given in Appendix D), the response function R_{ξ^2} can likewise be written as a sum of even angular harmonics. In this case, the expansion also ends up at the sixth harmonic

$$R_{\xi^2} = \frac{1}{h_q^2(h_q + \sin^2 \alpha)^4} \left(\chi_{\xi^2}^{(0)} + \chi_{\xi^2}^{(2)} \cos 2\alpha + \chi_{\xi^2}^{(4)} \cos 4\alpha + \chi_{\xi^2}^{(6)} \cos 6\alpha \right), \quad (53)$$

with the corresponding scattering function

$$S_{\xi^2} = \frac{\Lambda_q^4}{7560} \langle \tilde{I}_M^2 \rangle q^4 \xi^2. \quad (54)$$

The explicit expressions for the coefficients $\chi_{\xi^2}^{(n)}$ are given in Appendix C.

Owing to the prefactor h_q^{-2} , the response is strongly enhanced in the low-field regime and remains positive across all values in (t, α) parameter space. As $h_q \rightarrow 0$, the intensity increases rapidly, leading to pronounced maxima at small values of the reduced field parameter. The intensity is concentrated near $\alpha \approx 0$ and $\alpha \approx \pi$, where $\sin \alpha$ is small and the denominator $(h_q + \sin^2 \alpha)^4$ attains its minimal values. In contrast, the response is strongly suppressed around $\alpha = \pi/2$, where $\sin^2 \alpha = 1$ and the denominator is maximal. Unlike the linear response R_ξ , the function R_{ξ^2} does not possess a global angular line at which it vanishes for all h_q . Instead, its zeros form curved nodal lines in the (α, h_q) plane, arising from the mutual cancellation of several even angular harmonics.

As in the case of $R_{\xi\kappa}$, expansion formally contains harmonics up to $\cos 6\alpha$ but higher-order oscillations are efficiently suppressed and the overall angular dependence remains smooth.

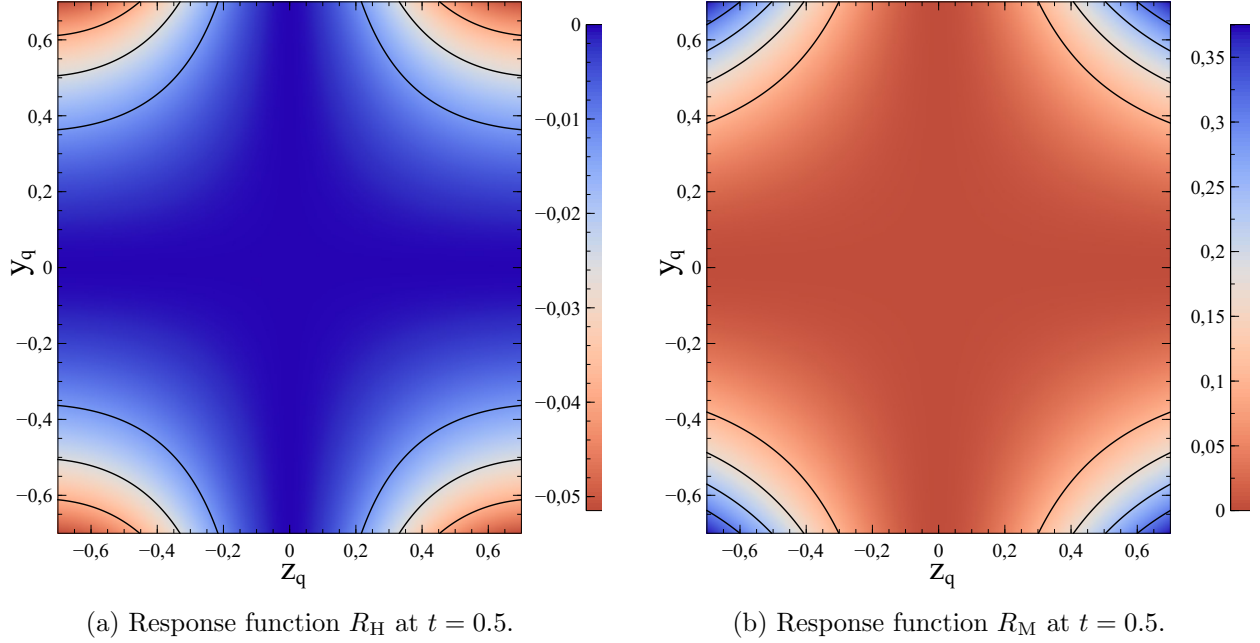


Figure 3: Two-dimensional maps of the standard (isotropic Heisenberg-type) response functions in (y_q, z_q) coordinates at the fixed reduced field parameter $t = h_q/(h_q + 1) = 0.5$. These plots serve as reference patterns for comparison with the anisotropic response functions shown in Fig. 4.

To facilitate direct comparison with experimental SANS data, we represent the response functions in detector-plane coordinates (z_q, y_q) rather than in angular variables. In typical SANS measurements, the intensity is recorded as a function of the Cartesian components of the scattering vector in the detector plane. The (z_q, y_q) representation therefore provides a more transparent visualization of the angular structure of the response functions from an experimental perspective.

The standard Heisenberg-type response functions R_H and R_M (as shown on fig.(3)) exhibit the characteristic angular anisotropy of magnetic SANS in the perpendicular geometry.

In contrast, the exchange-anisotropy-induced terms (shown on fig. (4)) display characteristic modifications of this pattern.

The detector-plane maps of R_M and R_ξ exhibit qualitatively similar angular structures, although their signs is opposite. While R_M reflects longitudinal magnetization fluctuations in the Heisenberg-like theory, the R_ξ arises from the linear anisotropic correction of the exchange. Consequently, linear correction of the symmetric exchange anisotropy does not introduce a fundamentally new angular symmetry, but rather redistributes the weight of angular harmonics already present in the Heisenberg-like response.

The mixed term $R_{\xi\kappa}$, represents the coupling between symmetric exchange anisotropy and random anisotropy fluctuations. It vanishes if either ξ or κ is zero and therefore constitutes a genuine interference term between two distinct sources of magnetic disorder.

The quadratic contribution R_{ξ^2} generates additional angular modulation. The intensity maxima are aligned predominantly along the vertical direction ($z_q \approx 0, |y_q|$ large), while suppression occurs near

the horizontal axis.

These features constitute experimentally accessible signatures of symmetric exchange anisotropy.

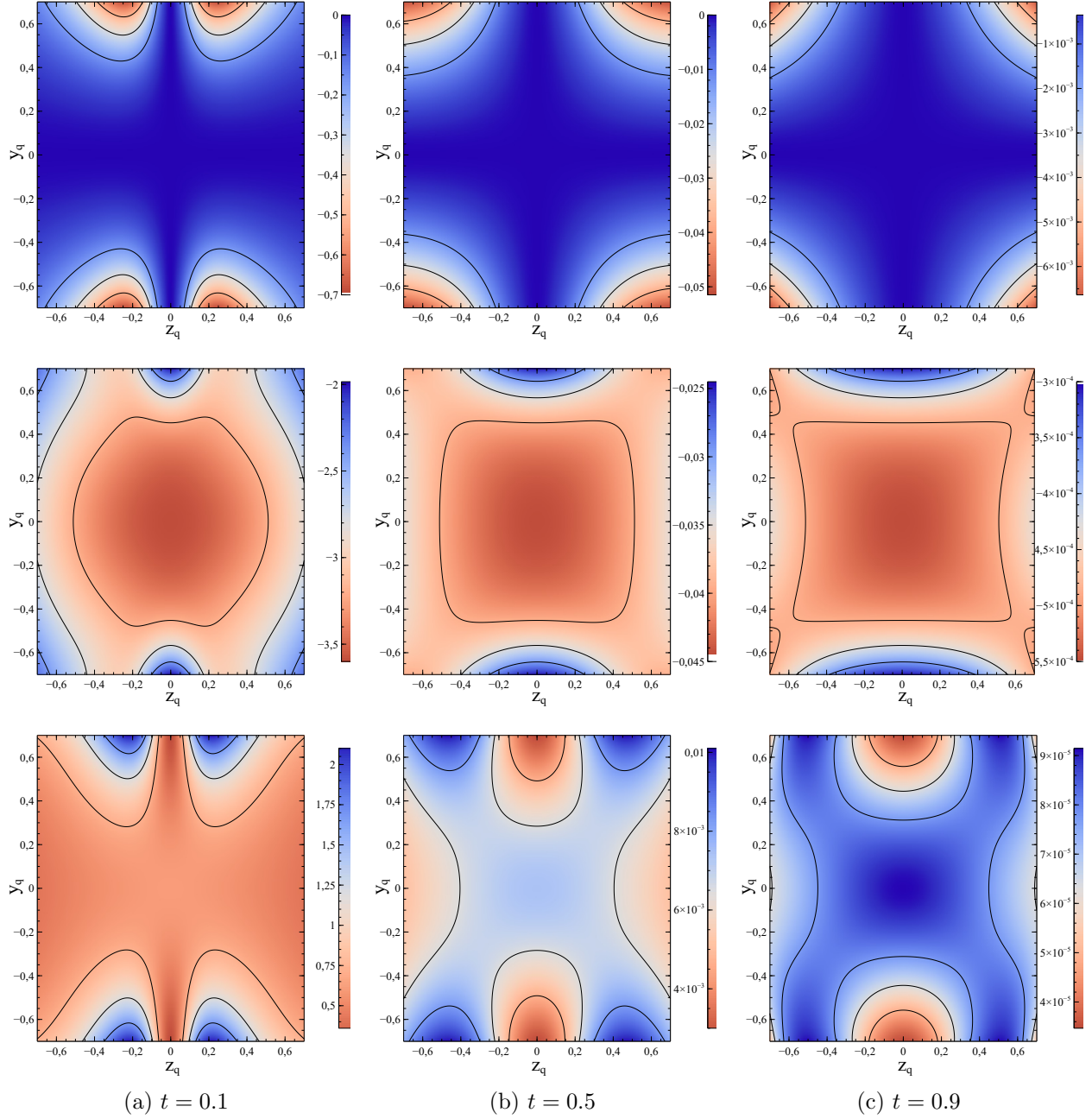


Figure 4: Two-dimensional maps of the anisotropic response functions in (y_q, z_q) coordinates at different values of the reduced field parameter $t = h_q/(h_q + 1)$. Top row: linear contribution R_ξ . Middle row: mixed contribution $R_{\xi\kappa}$. Bottom row: quadratic contribution R_{ξ^2} . Columns correspond to $t = 0.1$, $t = 0.5$, and $t = 0.9$, respectively. The evolution of the angular structure with increasing field illustrates the distinct symmetry properties and scaling behavior of the individual anisotropic terms.

7.2 Anisotropic SANS cross sections in parallel geometry

Substituting equations (33) and (34) into the expression for the magnetic SANS cross section in the parallel geometry and expanding in the small parameter ξ , the cross section again separates into Heisenberg-like and anisotropic contributions. In contrast to the perpendicular geometry, however, the contribution linear in the symmetric exchange anisotropy vanishes identically,

$$\left. \frac{d\Sigma_{\parallel}^M}{d\Omega} \right|_{\xi} = 0. \quad (55)$$

The leading anisotropic correction in parallel geometry is therefore given by the mixed term proportional to $\xi\kappa$. As in the perpendicular case, this contribution can be written in a compact form as a scalar product of two vectors, $\mathbf{u} = (u_X, u_Y)$ and $\Phi^{\parallel} = (\Phi_X^{\parallel}, \Phi_Y^{\parallel})$, where the components of Φ^{\parallel} are given by

$$\Phi_X^{\parallel} = -2h_q^{-2}y_q(K_{YZ}x_q - K_{XZ}y_q), \quad (56)$$

$$\Phi_Y^{\parallel} = 2h_q^{-2}x_q(K_{YZ}x_q - K_{XZ}y_q). \quad (57)$$

After performing the directional averaging over crystallite orientations, the corresponding contribution to the magnetic SANS cross section becomes isotropic in the detector plane and assumes the simple form

$$\left\langle \frac{d\Sigma_{\parallel}^M}{d\Omega} \right\rangle_{\xi\kappa} = -\frac{8\Lambda_q^2 q^2}{315h_q^2} \langle \tilde{I}_M^2 \rangle \xi\kappa. \quad (58)$$

The contribution proportional to ξ^2 is also isotropic. This follows from the absence of any preferred in-plane direction that could break the macroscopic rotational symmetry of the system in the detector plane for the parallel scattering geometry.

Discussion and Conclusions

The developed micromagnetic theory of magnetic small-angle neutron scattering consistently accounts for weak symmetric anisotropic exchange in centrosymmetric ferromagnets. The exchange interaction was formulated in terms of a general fourth-rank tensor that was subsequently separated into isotropic and deviatoric parts. This decomposition makes it possible to relate all anisotropic effects to the symmetry properties of the deviatoric part of the exchange tensor.

A compact expression derived for the exchange energy and corresponding effective field remains valid for spatially inhomogeneous saturation magnetization. In the linear response regime, the isotropic part of the exchange tensor reproduces the well-known Heisenberg-type SANS response, whereas all anisotropic corrections are governed exclusively by the deviator of the exchange tensor. In polycrystalline systems, these corrections persist even after directional averaging over crystallites with randomly distributed anisotropy axes, whereby the symmetry of the exchange tensor manifests itself in the observable angular dependencies.

For the case of hexagonal exchange symmetry, we have obtained explicit analytical expressions for the anisotropic response functions proportional to ξ , $\xi\kappa$, and ξ^2 . The corresponding two-dimensional SANS maps exhibit several characteristic features absent in Heisenberg-type theory, including sign reversals, nontrivial nodal curves in angle-field space, and the emergence of higher even angular

harmonics. Despite the presence of terms up to the sixth harmonic in the analytical expressions, the angular dependence remains smooth, indicating an efficient suppression of higher-order harmonics by geometrical and magnetostatic factors.

Inspection of the general expressions for the scattering cross sections (presented in a separate file) shows that the specific symmetry of the exchange tensor, or more precisely of its deviatoric part, does not determine the maximal angular harmonic. Instead, the role of symmetry is to enforce the vanishing of certain harmonics.

The maximal harmonic is governed by the geometry of the scattering cross section and by the particular contribution under consideration. For example, for the term proportional to ξ^2 , the maximal power of the function ΔK_{ij} is equal to two. Since the kernel K_{ij} can generate at most a second-order polynomial in the components of the scattering vector \mathbf{q} , the quantity $(\Delta K_{ij})^2$ produces terms of order q^4 . As a result, the maximal power of \mathbf{q} in the expression for the ξ^2 contribution to the cross section is eight, once the geometric prefactors originating from magnetostatics are taken into account. Consequently, the total maximal angular order of the cross section is twelve for any symmetry.

The presented formalism is readily extendable to other crystallographic symmetries. Obtained results establish a link between symmetric exchange anisotropy and experimentally observable features in magnetic SANS, offering a route to identify and quantify anisotropic exchange interactions in nanostructured magnetic materials.

A Exchange energy for spatially varying saturation magnetization

In the presence of spatially inhomogeneous saturation magnetization, the normalized magnetization vector entering the exchange energy density (6) must be replaced by $\mathbf{m} = \mathbf{M}/M_S$. Accordingly, the spatial derivative of the magnetization component m_α can be written as

$$\partial_\beta m_\alpha = \partial_\beta \left(\frac{M_\alpha}{M_S} \right) = \frac{1}{M_S} \partial_\beta M_\alpha - \frac{M_\alpha}{M_S^2} \partial_\beta M_S. \quad (59)$$

Noting that

$$\frac{\partial_\beta M_S}{M_S} = \partial_\beta \ln \left(\frac{M_S}{M_0} \right), \quad (60)$$

where M_0 is the average saturation magnetization, and the derivative $\partial_\beta m_\alpha$ can be rewritten in the form

$$\partial_\beta m_\alpha = \frac{1}{M_S} \left[\partial_\beta M_\alpha - M_\alpha \partial_\beta \ln \left(\frac{M_S}{M_0} \right) \right]. \quad (61)$$

This motivates the introduction of the modified derivative

$$\mathcal{D}_\beta M_\alpha = \partial_\beta M_\alpha - M_\alpha \partial_\beta \ln \left(\frac{M_S}{M_0} \right), \quad (62)$$

which allows one to express spatial derivatives of the normalized magnetization in a compact form,

$$\partial_\beta m_\alpha = \frac{1}{M_S} \mathcal{D}_\beta M_\alpha. \quad (63)$$

Using this definition, the exchange energy density can be written as

$$e_{\text{EX}} = \frac{1}{2M_S^2} \sum_{\alpha\beta\gamma\delta} C_{\alpha\beta\gamma\delta}(\mathbf{r}) (\mathcal{D}_\beta M_\alpha)(\mathcal{D}_\delta M_\gamma), \quad (64)$$

where $C_{\alpha\beta\gamma\delta}(\mathbf{r})$ is the symmetric exchange tensor. This form of the exchange energy density serves as the starting point for the derivation of the effective exchange field presented in Appendix B.

B Derivation of the effective exchange field

The effective exchange field follows from the functional derivative of the exchange energy density with respect to the magnetization. In micromagnetic theory it is defined as (Aharoni, 1996)

$$H_{\text{EX},\alpha} = -\frac{1}{\mu_0} \left[\frac{\partial e_{\text{EX}}}{\partial M_\alpha} - \partial_\beta \left(\frac{\partial e_{\text{EX}}}{\partial(\partial_\beta M_\alpha)} \right) \right]. \quad (65)$$

Fluctuations of the exchange stiffness contribute only to higher-order corrections in the magnetic SANS cross section (Metlov & Michels, 2015). Therefore, in the following derivation the exchange tensor is treated as a constant. We first evaluate the derivative with respect to $\partial_\beta M_\alpha$. According to the Appendix A, exchange energy density can be written in the form

$$e_{\text{EX}} = \frac{1}{2M_S^2} C_{\mu\nu\gamma\delta} (\mathcal{D}_\mu M_\nu)(\mathcal{D}_\gamma M_\delta), \quad (66)$$

which yields

$$\frac{\partial e_{\text{EX}}}{\partial(\partial_\beta M_\alpha)} = \frac{1}{2M_S^2} C_{\mu\nu\gamma\delta} \left[\frac{\partial(\mathcal{D}_\mu M_\nu)}{\partial(\partial_\beta M_\alpha)} (\mathcal{D}_\gamma M_\delta) + \frac{\partial(\mathcal{D}_\gamma M_\delta)}{\partial(\partial_\beta M_\alpha)} (\mathcal{D}_\mu M_\nu) \right]. \quad (67)$$

The operator $\mathcal{D}_\mu M_\nu$ depends on $\partial_\beta M_\alpha$ only when $\mu = \beta$ and $\nu = \alpha$, since

$$\mathcal{D}_\beta M_\alpha = \partial_\beta M_\alpha - M_\alpha \partial_\beta \ln \left(\frac{M_S}{M_0} \right). \quad (68)$$

It therefore follows that

$$\frac{\partial(\mathcal{D}_\mu M_\nu)}{\partial(\partial_\beta M_\alpha)} = \delta_{\mu\beta} \delta_{\nu\alpha}. \quad (69)$$

Substituting this result into Eq. (67), we obtain

$$\frac{\partial e_{\text{EX}}}{\partial(\partial_\beta M_\alpha)} = \frac{1}{2M_S^2} C_{\alpha\beta\gamma\delta} (\mathcal{D}_\gamma M_\delta) + \frac{1}{2M_S^2} C_{\mu\nu\alpha\beta} (\mathcal{D}_\mu M_\nu). \quad (70)$$

Upon relabeling dummy indices and using the symmetry of the exchange tensor $C_{\alpha\beta\gamma\delta} = C_{\gamma\delta\alpha\beta}$, this expression can be written in the compact form

$$\frac{\partial e_{\text{EX}}}{\partial(\partial_\beta M_\alpha)} = T_{\alpha\beta}, \quad T_{\alpha\beta} = \frac{C_{\alpha\beta\gamma\delta}}{M_S^2} \mathcal{D}_\delta M_\gamma. \quad (71)$$

The quantity $T_{\alpha\beta}$ plays a role analogous to the stress tensor in elasticity theory.

We now evaluate the derivative of the exchange energy density with respect to M_α . Since $\mathcal{D}_\beta M_\alpha$

contains the term $-M_\alpha \partial_\beta \ln(M_S/M_0)$, we obtain

$$\frac{\partial(\mathcal{D}_\beta M_\alpha)}{\partial M_\alpha} = -\partial_\beta \ln\left(\frac{M_S}{M_0}\right). \quad (72)$$

Proceeding analogously to the previous steps and again using the symmetry of the exchange tensor, one finds

$$\frac{\partial e_{\text{EX}}}{\partial M_\alpha} = -\left[\partial_\beta \ln\left(\frac{M_S}{M_0}\right)\right] T_{\alpha\beta}. \quad (73)$$

Collecting all contributions and substituting the results into Eq. (65), the effective exchange field can be written as

$$H_{\text{EX},\alpha} = \frac{1}{\mu_0} \left[\partial_\beta T_{\alpha\beta} + \left(\partial_\beta \ln\left(\frac{M_S}{M_0}\right) \right) T_{\alpha\beta} \right]. \quad (74)$$

This expression serves as a starting point in the derivation of the Fourier image of the effective field and subsequent solution of Browns equations.

C Expressions for the polynomials $\chi^{(n)}$

This appendix collects the explicit expressions for the field-dependent polynomials $\chi^{(n)}$ that appear in the Fourier harmonic expansions of the anisotropic response functions $R_{\xi\kappa}$ and R_{ξ^2} . These polynomials encode the dependence on the reduced field parameter h_q and determine the relative weights of the individual angular harmonics.

Polynomials entering the response function $R_{\xi\kappa}$

The response function $R_{\xi\kappa}$ is expanded in even angular harmonics up to $\cos 6\alpha$. The corresponding coefficients are given by

$$\chi_{\kappa\xi}^{(0)} = -10 - 36h_q - 70h_q^2 - 24h_q^3, \quad (75)$$

$$\chi_{\kappa\xi}^{(2)} = 15 + 48h_q + 45h_q^2 + 32h_q^3, \quad (76)$$

$$\chi_{\kappa\xi}^{(4)} = -6 - 12h_q + 22h_q^2 + 24h_q^3, \quad (77)$$

$$\chi_{\kappa\xi}^{(6)} = 1 + 3h_q^2. \quad (78)$$

Polynomials entering the response function R_{ξ^2}

The response function R_{ξ^2} also contains even angular harmonics up to $\cos 6\alpha$. The coefficients multiplying these harmonics are given by

$$\chi_{\xi^2}^{(0)} = 10 + 4h_q(12 + h_q(30 + h_q(20 + 9h_q))), \quad (79)$$

$$\chi_{\xi^2}^{(2)} = -15 + 2h_q(-32 + h_q(-48 + h_q(-26 + 17h_q))), \quad (80)$$

$$\chi_{\xi^2}^{(4)} = 2(3 + 2h_q(-2 + h_q)(-2 + h_q(2 + 3h_q))), \quad (81)$$

$$\chi_{\xi^2}^{(6)} = -1 - 6h_q^3(2 + 3h_q). \quad (82)$$

The higher angular harmonics present in R_{ξ^2} originate from the additional angular prefactors discussed in Sec. VIII.

D Expression for the ξ^2 part of the anisotropic cross section

This appendix provides the explicit expression for the contribution to the perpendicular magnetic SANS cross section that is quadratic in the exchange anisotropy parameter ξ . The result is obtained by expanding the general expressions derived in Sec. VI to second order in ξ and retaining only terms that contribute within the linearized micromagnetic approximation

$$\begin{aligned}
\left. \frac{d\Sigma_{\perp}^M}{d\Omega} \right|_{\xi^2} &= \frac{K_{XZ}^2}{h_q^2} - \frac{2y_q \left[h_q^2 K_{YY} K_{YZ} + (1 + h_q) K_{XY} K_{XZ} (h_q + y_q^2) \right] z_q}{h_q^2 (h_q + y_q^2)^2} \\
&+ \frac{\left[h_q^3 K_{YZ}^2 + (h_q K_{XY}^2 + h_q^2 (2K_{XY}^2 + 2K_{YY}^2 + K_{YZ}^2)) y_q^2 + (1 + 2h_q) K_{XY}^2 y_q^4 \right] z_q^2}{h_q^2 (h_q + y_q^2)^3} \\
&- \frac{2y_q \left[h_q K_{XY} K_{XZ} + 2h_q K_{YY} K_{YZ} + K_{XY} K_{XZ} y_q^2 \right] z_q^3}{h_q (h_q + y_q^2)^3} \\
&+ \frac{y_q^2 \left[h_q (2K_{XY}^2 + 3K_{YY}^2) + 2K_{XY}^2 y_q^2 \right] z_q^4}{h_q (h_q + y_q^2)^4}. \tag{83}
\end{aligned}$$

The expression above serves as the starting point for the directional averaging performed in Sec. VII and for the construction of the corresponding response function R_{ξ^2} discussed in the main text. For specific crystallographic symmetries, many terms in Eq. (83) vanish identically after directional averaging, leading to the compact harmonic expansions discussed in Sec. VIII.

Acknowledgements

The authors are grateful to Prof. Andreas Michels from the University of Luxembourg for careful reading of the manuscript and many valuable remarks.

Conflicts of interest: The authors declare that there are no conflicts of interest.

Data availability: In this theoretical work all the data (to reproduce figures and other results of the present study) are contained within the manuscript.

References

- Aharoni, A. (1996). *Introduction to the theory of ferromagnetism*. Oxford: Oxford University Press.
- Akhiezer, A. I., Bar'yakhtar, V. G. & Peletminskii, S. V. (1968). *Spin Waves*. Amsterdam: North-Holland Publishing Company. Translated from Russian Spinovye volny.
<https://archive.org/details/spinwaves0000akhi>
- Belashchenko, K. D. (2004). *Journal of Magnetism and Magnetic Materials*, **271**(1), 28–38.
- Metlov, K. L. & Michels, A. (2015). *Physical Review B*, **91**(5), 054404.
- Michels, A. (2014). *Journal of Physics: Condensed Matter*, **26**(38), 383201.

- Michels, A. (2021). *Magnetic Small-Angle Neutron Scattering: A Probe for Mesoscale Magnetism Analysis*. Oxford University Press.
- Michels, A., Mettus, D., Titov, I., Malyeyev, A., Bersweiler, M., Bender, P., Peral, I., Birringer, R., Quan, Y., Hautle, P., Kohlbrecher, J., Honecker, D., Fernández, J. R., Barquín, L. F. & Metlov, K. L. (2019). *Phys. Rev. B*, **99**, 014416.
<https://link.aps.org/doi/10.1103/PhysRevB.99.014416>
- Quan, Y., Kohlbrecher, J., Hautle, P. & Michels, A. (2020). *Journal of Physics: Condensed Matter*, **32**(28), 285804.
<https://doi.org/10.1088/1361-648X/ab80f8>
- Toga, Y., Ishioka, K. & Tsuchiura, H. (2018). *Physical Review B*, **98**(5), 054418.
- Zaporozhets, V. D., Oba, Y., Michels, A. & Metlov, K. L. (2022). *Journal of Applied Crystallography*, **55**(3), 592–600.